Applied Nanoscience
https://doi.org/10.1007/s13204-018-0771-3

ORIGINAL ARTICLE

Reversible structural changes of in situ prepared $As_{40}Se_{60}$ nanolayers studied by XPS spectroscopy

Oleksandr B. Kondrat[1] · R. M. Holomb[1] · A. Csik[2] · V. Takats[2] · M. Veres[3] · A. Feher[4] · T. Duchon[5] · K. Veltruska[5] · M. Vondráček[6] · N. Tsud[5] · V. Matolin[5] · K. C. Prince[7] · V. M. Mitsa[1]

Received: 2 January 2018 / Accepted: 10 April 2018

Abstract
$As_{40}Se_{60}$ nanolayers, as-deposited, annealed and in situ illuminated by green (532 nm) laser light, were studied using synchrotron radiation photoelectron spectroscopy. Changes in composition and local atomic coordination occurring in the irradiated region of $As_{40}Se_{60}$ films were monitored by analysis of As 3*d* and Se 3*d* core levels. It was found that the thermal treatment causes a decrease of the concentration of homopolar (As–As and Se–Se) bonds. On the other hand, an increasing concentration of both As-rich and Se-rich structural units (s.u.) with homopolar As–As and Se–Se bonds was observed under in situ green laser illumination of $As_{40}Se_{60}$ nanolayers. This process appeared to be reversible for a few sequences of annealing and illuminating of the sample. After a few cycles storing at ambient conditions the $As_{40}Se_{60}$ film composition was gradually changing, i.e. the aging effect was detected due to a drastic loss of As under ambient conditions. The surface local structure of the $As_{40}Se_{60}$ nanolayers and their photoinduced transformation are discussed in detail.

Keywords As–Se nanolayers · Photoinduced changes · Synchrotron radiation photoelectron spectroscopy · Core level · Valence band · Chalcogenide thin films

Introduction

Amorphous chalcogenides have been of great interest due to their remarkable structural, electronic and optical properties (Kolobov and Tominaga 2003; Zakery and Eliiott 2007; Stronski 1998). Many properties of chalcogenide glasses were found to be sensitive to near-bandgap light. Photons may influence optical, electrical, chemical, volume or mechanical properties of glasses (Tanaka 1990; Shimakawa et al. 1995). These changes can be transient, metastable or permanent. Based on these phenomena, i.e. light-sensitive properties of chalcogenide glasses and especially their amorphous thin films, numerous applications have been devised (Eisenberg et al. 1995; Kim et al. 1995; Stronski and Vlcek 2000; Sanghera and Aggarwal 1997). Of special interest among these is the development of high-quality optical elements for all optical signal processing systems. High-level integration of such elements into optical microdevices requires improved fabrication technology facilitating low optical losses at the near-surface layers and high damage threshold for femtosecond laser pulses. Consequently, the control over both structure and composition of light-sensitive materials is of utmost importance for rational design of future nanoelectronics and nanophotonics.

Arsenic selenide glasses are among the most important glassy chalcogenide materials. Different As_xSe_{100-x} compositions exhibit distinctive opto-mechanical properties (Krecmer et al. 1997). For example, it was previously found

✉ Oleksandr B. Kondrat
oleksandr.kondrat@uzhnu.edu.ua

1 Uzhhorod National University, Pidhirna Str. 46, Uzhhorod 88000, Ukraine

2 Institute for Nuclear Research, Hungarian Academy of Sciences, Debrecen 4001, Hungary

3 Wigner Research Centre for Physics, Hungarian Academy of Sciences, Budapest 1121, Hungary

4 Pavol Jozef Šafárik University in Košice, Park Angelinum 9, Košice, Slovak Republic

5 Department of Surface and Plasma Science, Faculty of Mathematics and Physics, Charles University, V Holešovičkách 2, 18000 Prague 8, Czech Republic

6 Institute of Physics, Academy of Science of the Czech Republic, Na Slovance 2, 182 21 Praha 8, Czech Republic

7 Elettra-Sincrotrone Trieste S.C.p.A, Area Science Park, Strada Statale 14, Km 163.5, 34149 Basovizza, TS, Italy

Published online: 19 April 2018

that $As_{50}Se_{50}$ exhibits high light sensitivity during photostructural transformations due to the presence of homopolar As–As bonds (Lyubin 1987; Pfeiffer et al. 1991). It is reasonable to expect the behavior to be modified for other As_xSe_{100-x} compositions with respect to their optical band gap and concentration of the homopolar As–As bonds.

Here, we focus on $As_{40}Se_{60}$, where the deficiency of As with respect to $As_{50}Se_{50}$ leads to a decrease of the optical band gap (from 1.95 to 1.90 eV for bulk $As_{50}Se_{50}$ and $As_{40}Se_{60}$, respectively) (Hammam et al. 1985). Stoichiometric $As_{40}Se_{60}$ also has the interesting feature of having a composition exactly at the floppy-to-rigid transition (Phillips 1981). We examine structural changes of in situ fabricated $As_{40}Se_{60}$ nanolayers during thermal annealing and illumination by monochromatic coherent light with near-bandgap energy via photoelectron spectroscopy. The influence of the exposure to ambient conditions, pertinent to real-life applications, on the structural stability was also studied.

Experimental details

High optical quality glass was used as source material for in situ deposition to avoid any contamination (carbon, oxygen, etc.). The bulk $As_{40}Se_{60}$ samples were obtained by the conventional melt-quenching route in evacuated quartz ampoules from a mixture of high purity 99.999% As and Se precursors (Kondrat et al. 2012a). The arsenic triselenide nanolayers were prepared in situ by ordinary thermal evaporation of bulk glass powder from a ceramic crucible at a temperature of 220 °C and deposition onto silicon substrates directly in the preparation chamber of the Materials Science Beamline (MSB, Elettra synchrotron) using standard available equipment, similarly to the As–S films in Kondrat et al. (2015a). After deposition the samples were transferred to the analyzer chamber in the ultra-high vacuum (UHV) (i.e. without contact with air). Thermal annealing of the prepared films was performed at a temperature of $T_{an} \sim 100$ °C for 0.5 h in the analyzer chamber. This temperature was chosen on the basis of preliminary investigations. It was found that further increasing of annealing temperature leads to changes of the shape and intensity of the As 3*d* peak, indicating the structure of the film was damaged. A green diode laser operating at 532 nm wavelength (corresponding to photon energy of ~ 2.33 eV) was used to investigate the influence of over-bandgap irradiation on the structure of $As_{40}Se_{60}$ (bandgap $E_g \sim 1.85$ eV) nanolayers. Laser intensity and exposure time were chosen based on our previous investigations of As–Se glasses by means of Raman spectroscopy. The light source was outside the vacuum chamber and the maximum intensity of laser light was 55 mW/cm^2. The fused silica window of the chamber had a transmission for the laser light of about 0.92. The optical irradiation was carried out with 50 mW/cm^2 intensity on the sample and 0.5 h exposure time in situ, in the UHV system at room temperature, right after the film deposition, i.e. there was no contact of the sample with air. When several thermal and light illumination treatments were applied to the samples, they were performed with the same conditions.

Photoemission spectroscopy measurements of As 3*d* and Se 3*d* core levels were carried out with primary photon energy of 160 eV in normal emission geometry (Briggs and Seah 1993). In addition, 650 eV primary photon energy was used for compositional analysis and depth profiling of the nanolayers. Photoemission spectra were recorded using the PHOIBOS 150 multi-channel hemispherical analyzer with energy step of 0.05 eV and pass energy of 2 eV. The As 3*d* and Se 3*d* core level spectra of $As_{40}Se_{60}$ films were measured with total (photon beam + analyser + natural line width, measured as the width of the Fermi edge) energy resolution of 0.35 eV. Elettra operates in top-up mode, providing a very stable flux, so normalization to ring current was not necessary. The As 3*d* and Se 3*d* spectra were fitted using Voigt functions with a Shirley-type background to yield peak position and intensity. The quantitative analysis based on the acquired intensities was carried out with respect to the photon flux and atomic photoionization cross-section (Yeh 1993). The fitting procedure is described in detail in Kondrat et al. (2012b). In addition to core level spectra, valence band (VB) spectra of as-deposited and treated $As_{40}Se_{60}$ nanolayers were measured with primary photon energy of 30 eV.

Apart from this, XPS spectra of as-deposited and aged (exposure to ambient conditions for 1 week and 1 year) $As_{40}Se_{60}$ films were measured at the surface physics laboratory (SPL, Charles University, Prague, Czech Republic) and materials science laboratory (Institute for Nuclear Research, Debrecen, Hungary). An X-ray source with Al K_α anode (excitation energy of 1486.6 eV) in combination with PHOIBOS 150 multi-channel hemispherical analyzer were used for acquisition of As 3*d*, Se 3*d*, C1*s* and O 1*s* core levels in normal emission geometry.

Results and discussion

Stoichiometry and component analysis of $As_{40}Se_{60}$ nanolayers

Survey synchrotron radiation excited photoelectron spectroscopy (SRPES) scans of the samples (not shown) indicated the presence of silicon (very low intensity), arsenic and selenium only. The Se 3*d* and As 3*d* core level spectra of as-deposited, annealed and illuminated $As_{40}Se_{60}$ nanolayers together with the results of curve fitting are shown in Fig. 1. The Se 3*d* core level (Fig. 1a) was decomposed into two doublets with $3d_{5/2}$ spin–orbit splitting components at

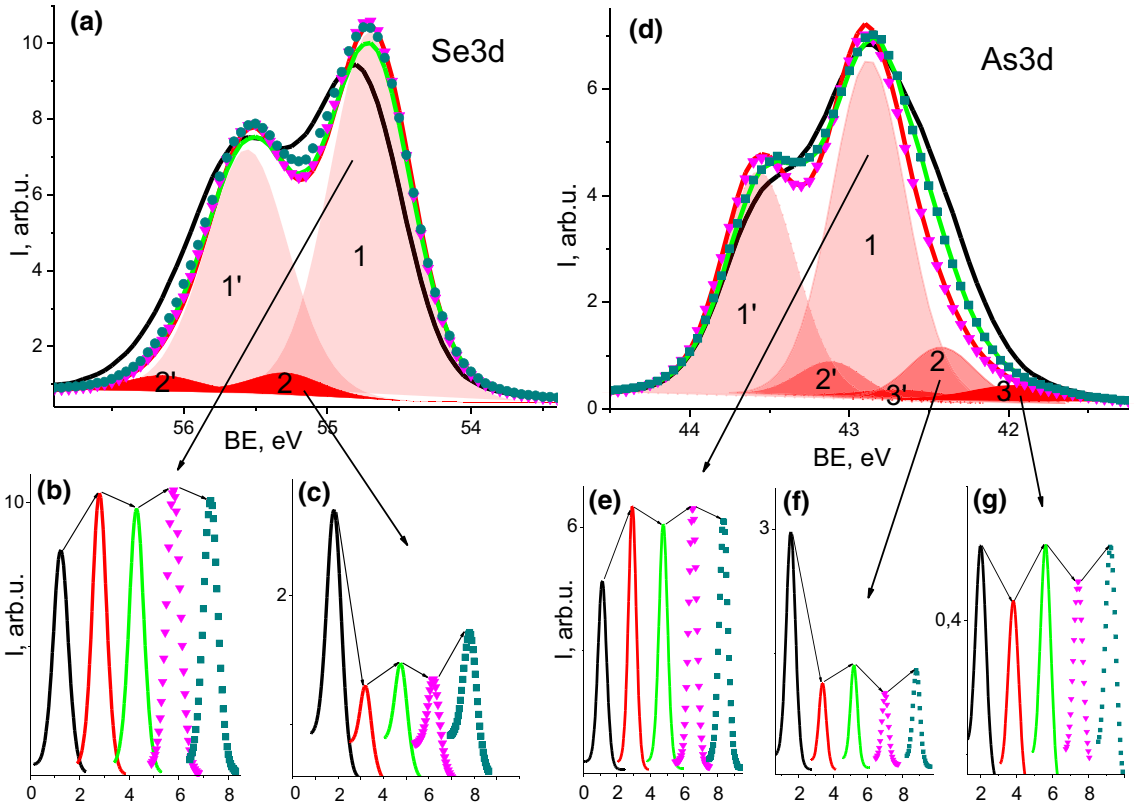

Fig. 1 Se 3*d* (**a**) and As 3*d* (**d**) core level spectra of $As_{40}Se_{60}$ nanolayers: as-deposited (black lines), 1st annealed (red lines), 1st illuminated (green lines), 2nd annealed (pink triangles), and 2nd illuminated (dark green squares), together with results of typical curve fitting. 1 and 1′ denote $3d_{5/2}$ and $3d_{3/2}$ components of Se–As_2 s.u. of the Se 3*d* spectrum (**a**) and As–Se_3 s.u. of As 3*d* spectrum (**d**), respectively. 2 and 2′ denote $3d_{5/2}$ and $3d_{3/2}$ components of Se–SeAs s.u. of the Se 3*d* spectrum (**a**) and As–Se_2As s.u. of As 3*d* spectrum (**d**), respectively. 3 and 3′ denote $3d_{5/2}$ and $3d_{3/2}$ components of As–$SeAs_2$ s.u. of the As 3*d* spectrum (**d**), respectively. Lower panels demonstrate the changes of the contributions of Se $3d_{5/2}$ and As $3d_{5/2}$ peak components after the each step of treatment (as-deposited → annealed → illuminated → annealed → illuminated): Se–As_2 (**b**), Se–SeAs (**c**), As–Se_3 (**e**), As–Se_2As (**f**) and As–$SeAs_2$ (**g**). For better understanding position of each component are separated in space with the step of 1.6

binding energy (BE) of ~ 54.8 eV (peak 1) and ~ 55.2 eV (peak 2). According to our calculations (Kondrat et al. 2015b) and previously published experimental data for the As_2Se_3 crystal (Choi et al. 2007; Petkov et al. 1994), peak 1 originates from the presence of the stoichiometric Se–As_2 s.u. on the surface of $As_{40}Se_{60}$ nanolayers. DFT calculations showed that substitution of As by Se leads to an energy shift of the Se 3*d* core level to 55.3 eV for a Se–SeAs s.u. and to 55.7 eV for a Se–Se_2 s.u. Thus, peak 2 indicates the presence of Se–SeAs s.u. in the structure of the nanolayers.

The As 3*d* core level spectra (Fig. 1d) of the as-deposited, annealed and illuminated $As_{40}Se_{60}$ nanolayers, were fitted using three components. These were assigned to arsenic bonded to three selenium atoms (As–Se_3 s.u., ~ 42.9 eV, peak 1), arsenic bonded to two selenium and one arsenic atom (As–Se_2As s.u., ~ 42.4 eV, peak 2) and arsenic bonded to one selenium and two arsenic atoms (As–$SeAs_2$ s.u., ~ 42.0 eV, peak 3). The energies of peaks 2 and 1 are in good agreement with values reported for materials with corresponding arsenic chemical coordination: realgar-type As_4Se_4, and As_2Se_3, respectively (Wanger et al. 1979; Sarode et al. 1979; Ueno 1983). The calculated molecular orbital energy of the As 3*d* core level components for structural units, where Se was substituted by As in $AsSe_3$ pyramids (i.e. As–Se_2As and As–Se_3), is in general agreement with the experimental data (Kondrat et al. 2015b). We, therefore, assign the peak at ~ 42.0 eV (peak 3) to the As–$SeAs_2$ s.u.

The results of As 3*d* and Se 3*d* core level fitting of the SRPES spectra are summarized in Table 1. As can be seen, the shapes of peak components are different while their BEs are nearly the same and correlate well with published DFT calculations and experimental data (Kondrat et al. 2015b; Wanger et al. 1979; Sarode et al. 1979; Ueno 1983; Briggs and Seah 1993; Ueno and Odajima 1981; Bahl et al. 1976).

The As and Se atomic concentration, As–Se ratio, and percentages of the Se 3*d* and As 3*d* peak components relative to the total intensity of the corresponding core level spectra of the $As_{40}Se_{60}$ nanolayers at each step of investigation are

Table 1 Binding energies (BE, ±0.1 eV) and full width at half maximum (FWHM) (±0.05 eV) data of individual components determined from curve fitting of Se 3*d* and As 3*d* SRPES spectra of as-deposited, annealed and illuminated by green ($\lambda = 532$ nm) laser $As_{40}Se_{60}$ nanolayers

Core level/component	As-deposited		1st annealed		1st illuminated		2nd annealed		2nd illuminated	
	BE	FWHM	BE	FWHM	BE	FWHM	BE	FWHM	BE	FWHM
Se 3*d*										
$Se–As_2$	54.8	0.7	54.7	0.7	54.7	0.7	54.7	0.7	54.7	0.7
Se–SeAs	55.2	0.7	55.3	0.6	55.2	0.6	55.3	0.6	55.2	0.7
As 3*d*										
$As–Se_3$	42.9	0.6	42.9	0.6	42.8	0.6	42.9	0.6	42.8	0.6
$As–Se_2As$	42.4	0.6	42.4	0.5	42.4	0.5	42.4	0.4	42.4	0.5
$As–SeAs_2$	42.0	0.7	42.0	0.7	42.0	0.7	42.0	0.6	42.0	0.7

calculated and listed in Table 2. As can be seen, the As/Se ratio of the as-deposited $As_{40}Se_{60}$ nanolayers is very close to that in bulk glass. The first thermal annealing of the sample at $T_{an} \sim 100$ °C for 0.5 h in UHV leads to a 2% decrease of the arsenic content, which is then partially restored (increase of 1.3%) during in situ illumination of the sample by green laser. The same trend is kept during the second cycle, with a 2% decrease during the thermal treatment and a 1.2% increase during the in situ illumination. The As depletion and enrichment is connected with structural changes that occur in the sample surface during the in situ cycles of thermal treatment and laser illumination and can be elaborated upon through a detailed component analysis.

The main component of the Se 3*d* peak of as-deposited $As_{40}Se_{60}$ nanolayers is the $Se–As_2$ s.u., with a significant (~21%) contribution of the Se–SeAs s.u. (see Table 2). Such substantial content of homopolar Se–Se bonds in a nominally stoichiometric $As_{40}Se_{60}$ is balanced by a corresponding quantity of the As–As bonds ($As–Se_2As$ and $As–SeAs_2$ s.u.) detected in As 3*d* core levels of as-deposited film apart from the $As–Se_3$ s.u. (Table 2). The presence of the homopolar bonds was described in our previous publications for the films of As–Se system (Kondrat et al. 2017b), for example) and for the As_2S_3 films (Kondrat et al. 2017a), being isostructural with the $As_{40}Se_{60}$ composition. Specifically, thermal evaporation of the glass source material can lead to fragmentation, and consequently to deposition of clusters containing homopolar bonds. Such fragmentation has been previously observed in a mass spectrometry study (Mott and Davis 1979) of the As–S system, where the presence of S_2 and different AsS particles was revealed. We expect the same processes to play a role in the generation of homopolar bonds during deposition of the $As_{40}Se_{60}$ nanolayers.

Thermal annealing causes ordering of the structure, i.e. a significant decrease in the homopolar bonds. This can be rationalized as thermally induced formation of pyramidal structural units from constituents of the homopolar bonds. On the other hand, in situ illumination of $As_{40}Se_{60}$ nanolayers by green laser light partially restores the homopolar Se–Se and As–As bonds (Fig. 1; Table 2). Similar As–As bonds formation was observed in As_2S_3 film during in situ over-bandgap laser illumination (Kondrat et al. 2015a). As discussed there, the energy transfer from the excited electrons to the atoms plays a crucial role in photostructural transformations. It causes bond breaking and/or bond switching and glass network transformations accompanied by atomic movement. Such mechanism can also account for the additional homopolar As–As bond formation and the induced topological disorder. Specifically, over-bandgap laser illumination causes As-enrichment of the nanolayers' surface due to the transformation of the glass network by atomic movement of As from deeper layers toward the

Table 2 Atomic concentrations, As/Se ratio (the values of As/Se ratio for the bulk glasses are given in parentheses for comparison), and contribution (area, ±5%) to the core level of each doublet of individual components determined from curve fitting of Se 3*d* and As 3*d* SRPES spectra of the $As_{40}Se_{60}$ nanolayers

Element/core level/component	As-deposited	1st annealed	1st illuminated	2nd annealed	2nd illuminated
As, %	39.6	37.4	38.7	36.5	37.8
Se, %	60.4	62.6	61.3	63.5	62.2
As/Se	0.66 (0.67)	0.60	0.63	0.57	0.61
Se 3*d*					
$Se–As_2$, %	78.9	95.4	93.2	96.1	91.0
Se–SeAs, %	21.1	4.6	6.8	3.9	9.0
As 3*d*					
$As–Se_3$, %	62.7	83.9	80.6	86.6	81.8
$As–Se_2As$, %	31.8	11.2	13.3	9.1	12.4
$As–SeAs_2$, %	5.5	4.9	6.1	4.3	5.8

surface (Kondrat et al. 2017a). Further in situ annealing and illumination repeat the processes of glass network transformations (i.e. decreasing and increasing of Se–Se and As–As homopolar bonds, respectively).

It should be noted that Kovalskiy et al. have obtained interesting results described in Kovalskiy et al. (2017). These authors investigated the influence of UV-irradiation in air and argon atmosphere on the structure of arsenic sulfide films, isostructural to the As–Se system. These authors noticed that $As_{40}S_{60}$ thin film irradiation by non-polarized LED light with wavelength 525 nm decreases the number of both S–S and As–As homopolar bonds in the structure of films, but using light source with wavelength 375 nm leads to complete disappearance of the s.u. with As–As bonds and significant increase of the s.u. with S–S homopolar bonds. The S/As ratio increases too. A similar decrease of homopolar bonds in the structure of $As_{40}S_{60}$ thin films under near-bandgap light illumination in ambient conditions were described in Kondrat et al. (2017a). However, the in situ experiment (Kondrat et al. 2015a) demonstrated a decrease of the S–S bonds and increase of As–As bonds in the structure of the $As_{40}S_{60}$ thin film under the blue (405 nm) laser illumination. Moreover, illumination of thermally deposited $As_{40}Se_{60}$ thin film by near-bandgap laser light in air leads to formation additional Se–Se bonds and a significant decrease of As–As bonds (Kondrat et al. 2012b) which is contradictory to the present results. All these facts allow us to conclude that the carbon–oxygen layer(s) on the surface of films, adsorbed during contact with the air, affects the photostimulated processes on the near-surface layers of films.

The shape of the As 3*d* core levels after the 1st and 2nd annealing is almost identical (see Fig. 1), as are the As 3*d* spectra of the illuminated samples. We conclude that the process of in situ formation and breaking of the homopolar bonds in the structure of the $As_{40}Se_{60}$ nanolayers by annealing and over-bandgap laser illumination is cyclic, and structural changes are reversible. This phenomenon can be used for the in situ control of the structure and, consequently, the properties of the $As_{40}Se_{60}$ nanolayers. We highlight this as an important feature for practical applications in modern nanoelectronics, all optical signal processing, etc.

Valence band spectra of As–Se nanolayers

In addition to core level measurements, synchrotron radiation excited valence band spectra of $As_{40}Se_{60}$ nanolayers were also acquired, and are shown in Fig. 2.

The overall shape of the spectra is similar and correlates well with our previous results (Kondrat et al. 2015a, b). Only the valence band spectrum of the as-deposited $As_{40}Se_{60}$ nanolayers differs from the others, exhibiting a valley at ~ 5 eV. This distinction can be straightforwardly rationalized by the above-discussed variations observed of the

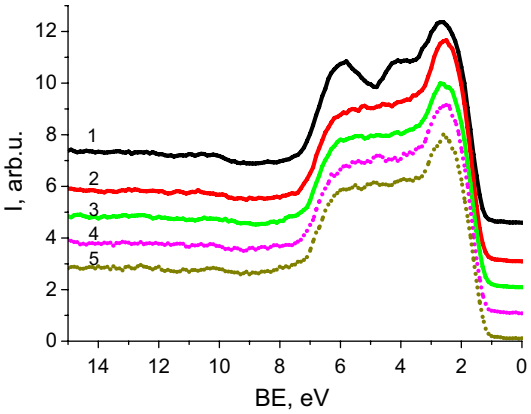

Fig. 2 Valence band spectra of the $As_{40}Se_{60}$ nanolayers: as-deposited (1, black line), 1st annealed (2, red line), 1st illuminated (3, green line), 2nd annealed (4, pink dots), and 2nd illuminated (5, dark green dots)

corresponding core levels. Kovalskiy et al. (2008) pointed out that the top of the VB of $As_{35}S_{65}$ amorphous thin films (isostructural to the As–Se system) is formed by lone-pair 3*p* electrons of sulfur, and the next part of the VB is formed by As 4*p* and S 3*p* (bonding electrons). Our previous DFT calculations (Kondrat et al. 2015b) have established that the top of the valence band (6–7 eV) of amorphous As–Se system is formed by Se-centered s.u. (Se–Se_2, Se–SeAs, and Se–As_2), whereas the region of ~ 4–5 eV is affected mainly by As-centered s.u. The maximum at ~ 4 eV thus indicates enrichment of the structure by As–As bonds, while the peak at ~ 6 eV points to additional Se–Se bonds. The VB spectra confirm the excess of s.u. with homopolar bonds found in As 3*d* and Se 3*d* core levels of as-deposited nanolayers. Further treatments stabilize the structure of the nanolayers.

Aging effect

For the practical applications of the nanolayers formed by As and Se atoms (Shchurova et al. 2006), it is necessary to know the stability of the material at ambient conditions. For this reason, the aging of $As_{40}Se_{60}$ nanolayers was studied. It should be noted that the experiments were carried out with a conventional XPS source and with a lower, but still sufficient, resolution. The $As_{40}Se_{60}$ nanolayers were deposited onto silicon substrates and annealed in situ. Then the As 3*d*, Se 3*d*, C 1*s* and O 1*s* core level spectra of the annealed samples were acquired. Next, the sample was removed from the UHV chamber and was stored at ambient conditions. The measurements were repeated after 1 week and 1 year of storage. Results are shown in Fig. 3. Regarding the C 1*s* core level, only the C–C and C–O components were detected for films aged for 1 week and 1 year (data not shown).

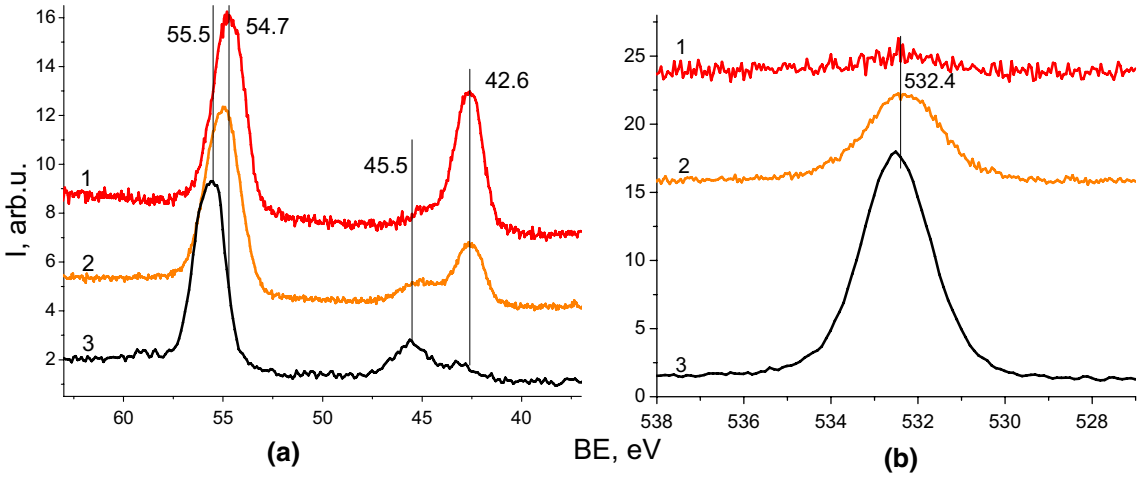

Fig. 3 Se 3*d* and As 3*d* (**a**) and O 1*s* (**b**) core level spectra of $As_{40}Se_{60}$ thin films, annealed (1, red lines), aged for 1 week (2, orange lines) and aged for 1 year (3, black lines)

The Se 3*d* core level of $As_{40}Se_{60}$ nanolayers annealed in UHV is centered at 54.7 eV, which is indicative of the dominance of stoichiometric Se–As_2 s.u. The corresponding As 3*d* core level spectrum is centered at 42.6 eV. This binding energy can be explained by overlapping As–Se_3 (~42.9 eV), As–Se_2As (~42.4 eV) and As–$SeAs_2$ (~42.0 eV) structural units. These results correlate well with the SRPES measurements described in previous sections. As expected, oxygen (Fig. 3b, curve 1) and carbon (not shown here) were almost undetectable in the as-prepared nanolayers. After aging the nanolayers for 1 week at ambient conditions the Se 3*d* core level noticeably shifts towards higher binding energy (Fig. 3a, curve 2). The shift can be explained by development of the Se–Se s.u., which is corroborated by a significant decrease of As 3*d* core level intensity, i.e. the quantity of arsenic in the structure decreased. Apart from this, a shoulder appeared at 45.5 eV and it indicates the presence of arsenic oxide (Wanger et al. 1979). It correlates with the appearance of the peak at 532.4 eV in O 1*s* core level spectra (Fig. 3b, Wanger et al. 1979; King et al. 1990). This process continued during further exposure to air for 1 year. The As 3*d* peak almost disappears, but the shoulder at 45.5 eV increases in intensity (Fig. 3a, curve 3), i.e. the amount of arsenic oxide increases in the structure of the $As_{40}Se_{60}$ thin film. Due to the deficit of As, the Se–As bonds were broken, and selenium reverted to Se–Se homopolar bonds, as understood from the Se 3*d* peak position at 55.5 eV (Wanger et al. 1979). Similar drastic loss of As on the surface of the two As-rich $As_{40}Se_{60}$ and $As_{50}Se_{50}$ compositions was detected in our previous investigations (Kondrat et al. 2012a, b) and explained by the presence of homopolar As–As bonds in the structure of As–Se films. These weak As–As bonds in the surface region can easily break under the influence of ambient conditions, i.e. oxidation, etc. The oxidation of As leads to formation of As_2O_3 at the surface, and the desorption of volatile arsenic oxides from the top layers of the structure (Janai et al. 1978) can explain the drastic loss of As content. In parallel, diffusion takes place as well, and leads to penetration of some As–O species into the structure (Kondrat et al. 2012b). Due to this some quantity of arsenic oxide is detected.

Based on these results, we conclude that a protecting layer that prevents the loss of As from the structure is required for a practical use of the material.

Conclusions

$As_{40}Se_{60}$ nanolayers were studied in situ by synchrotron radiation photoelectron spectroscopy. Structural properties of $As_{40}Se_{60}$ nanolayers were examined during different types of treatments: the as-deposited samples were annealed and illuminated by green laser light. Calculated As/S ratio and atomic concentrations obtained from photoelectron spectra show that the stoichiometry of the as-deposited samples is very close to that of the bulk glass, but the nanolayers contain some homopolar As–As and Se–Se bonds. Thermal annealing of $As_{40}Se_{60}$ nanolayers leads to ordering of the structure, i.e. to a decrease of the concentration of homopolar bonds and to the formation of stoichiometric Se–As_2 and As–Se_3 s.u. In situ over-bandgap illumination stimulates diffusion processes in $As_{40}Se_{60}$ nanolayers. This leads to the formation of new s.u. with Se–Se and As–As bonds. Processes of structural ordering and homopolar bond formation are found to be reversible. Thermal annealing and over-bandgap laser illumination can be used to control the chemical structure and properties of $As_{40}Se_{60}$ nanolayers. Valence band spectra were found to be very similar for all

samples and were not as sensitive to the induced structural changes as core level spectra. Investigation of the influence of ambient conditions on the structure and properties of $As_{40}Se_{60}$ nanolayers showed drastic loss of As content due to formation and desorption of As–O s.u. For a practical use, the surface of the As–Se films should be protected by a buffer layer.

Acknowledgments OK, RH and VM gratefully acknowledge support from the Hungarian Academy of Sciences within the Domus Hungarica Scientiarum et Artium. CERIC-ERIC consortium and Czech Ministry of Education (LM2015057) are acknowledged for financial support. The work was carried out within the framework of the DB-884 Project of the Ministry of Education and Science of Ukraine. The publication contains the results of research conducted with the grant support of the State Fund for Fundamental Research under the Competitive Project 0117U006384. Authors are also acknowledging the GINOP-2.3.2-15-2016-00041 project, which is co-financed by the European Union and the European Regional Development Fund.

Compliance with ethical standards

Conflict of interest On behalf of all authors, the corresponding author states that there is no conflict of interest.

References

Bahl MK, Woodall RO, Watson RL, Irgolic KJ (1976) Relaxation during photoemission and LMM Auger decay in arsenic and some of its compounds. J Chem Phys 64:1210–1218

Briggs D, Seah MP (1993) Practical surface analysis, vol 1, 2nd edn. Wiley, New York

Choi DY, Madden S, Rode A, Wang R, Luther-Davies B (2007) Nanoscale phase separation in ultrafast pulsed laser deposited arsenic trisulfide (As_2S_3) films and its effect on plasma etching. J Appl Phys 102:083532–083535

Eisenberg NP, Manevich M, Klebanov M, Shutina S, Lyubin V (1995) Fabrication of microlens array for the IR by lithographic processes using an inorganic chalcogenide photoresist. Proc SPIE Int Soc Op Eng 2426:235–241

Hammam M, Adriaenssens GJ, Grevendonk W (1985) Steady-state photoconductivity in amorphous arsenic selenide compounds. J Phys C Solid State Phys 18:2151–2160

Janai M, Rudman PS, Mandelbaum F (1978) Mass spectrometric analysis of arsenic trisulfide. J Non Cryst Solids 27:67–73

Kim HM, Jeong JW, Kwak CH, Lee SS (1995) Binary phase spatial modulation using photoinduced anisotropy in amorphous As_2S_3 thin films. Appl Opt 34:6008–6011

King DE, Fernandez JE, Swartz WE (1990) An XPS study of the doping of trans, trans-*p*-distyrylbenzene with AsF5: a model conducting polymer system. Appl Surf Sci 45:325–339

Kolobov AV, Tominaga J (2003) Chalcogenide glasses as prospective materials for optical memories and optical data storage. J Mater Sci Mater Electron 14:677–680

Kondrat O, Popovich N, Holomb R, Mitsa V, Lyamayev V, Tsud N, Cháb V, Matolín V, Prince KC (2012a) Laser induced changes of $As_{50}Se_{50}$ nanolayers studied by synchrotron radiation photoelectron spectroscopy. J Thin Solid Films 520:7224–7229

Kondrat O, Popovich N, Holomb R, Mitsa V, Lyamayev V, Tsud N, Cháb V, Matolín V, Prince KC (2012b) Synchrotron radiation photoelectron spectroscopy studies of self-organization in $As_{40}Se_{60}$ nanolayers stored under ambient conditions and after laser irradiation. J Non Cryst Solids 358:2910–2916

Kondrat O, Holomb R, Popovich N, Mitsa V, Veres M, Csik A, Feher A, Tsud N, Vondráček M, Matolín V, Prince KC (2015a) In situ investigations of laser and thermally modified As_2S_3 nanolayers: synchrotron radiation photoelectron spectroscopy and density functional theory calculations. J Appl Phys 118:225307

Kondrat O, Holomb R, Popovich N, Mitsa V, Veres M, Csik A, Tsud N, Matolín V, Prince KC (2015b) Local surface structure and structural properties of As–Se nanolayers studied by synchrotron radiation photoelectron spectroscopy and DFT calculations. J Non Cryst Solids 410:180–185

Kondrat O, Holomb R, Csik A, Takats V, Veres M, Mitsa V (2017a) Coherent light photo-modification, mass transport effect and surface relief formation in As_xS_{100-x} nanolayers: absorption edge, XPS and Raman spectroscopy combined with profilometry study. Nanoscale Res Lett 12:149. https://doi.org/10.1186/s11671-017-1918-y

Kondrat O, Holomb R, Mitsa V, Veres M, Tsud N (2017b) Structural investigation of As–Se chalcogenide thin films with different compositions: formation, characterization and peculiarities of volume and near-surface nanolayers. Funct Mater 24(4):547–554

Kovalskiy A, Neilson JR, Miller AC, Miller FC, Vlcek M, Jain H (2008) Comparative study of electron- and photo-induced structural transformations on the surface of $As_{35}S_{65}$ amorphous thin films. Thin Solid Films 516:7511–7518

Kovalskiy A, Vlcek M, Palka K, Buzek J, York-Winegar J, Oelgoetz J, Golovchak R, Shpotyuk O, Jain H (2017) Structural origin of surface transformations in arsenic sulfide thin films upon UV-irradiation. Appl Surf Sci 394:604–612

Krecmer P, Moulin AM, Stephenson RJ, Rayment T, Welland ME, Elliott SR (1997) Reversible nanocontraction and dilatation in a solid induced by polarized light. Science 277:1799–1802

Lyubin VM (1987) Photostructural changes in chalcogenide glasses. J Non Cryst Solids 97–98:47–54

Mott NF, Davis EA (1979) Electronic processes in non-crystalline materials. Clarendon Press, Oxford

Petkov K, Krastev V, Ts Marinova (1994) XPS study of amorphous As_2S_3 films deposited onto chromium layers. Surf Interface Anal 22:202–205

Pfeiffer G, Paesler MA, Agarwal SG (1991) Reversible photodarkening of amorphous arsenic chalcogens. J Non Cryst Solids 130:111–143

Phillips JC (1981) Topology of covalent non-crystalline solids. 2. Medium-range order in chalcogenide alloys and a-Si(Ge). J Non Cryst Solids 43:37–77

Sanghera JS, Aggarwal ID (1997) Development of chalcogenide fiber optics at NRL. J Non Cryst Solids 213, 214:63–67

Sarode PR, Rao KJ, Hegd MS, Rao CNR (1979) Study of As2(Se, Te)3 glasses by X-ray absorption and photoelectron spectroscopy. J Phys C Solid State Phys 12:4119–4128

Shchurova TN, Savchenko ND, Kondrat AB, Opachko II (2006) Auger analysis and simulation of electronic states for $Ge_{33}As_{12}Se_{55}$–*p*-Si heterojunction. Surf Interface Anal 38(4):448–451

Shimakawa K, Kolobov A, Elliott SR (1995) Photoinduced effects and metastability in amorphous semiconductors and insulators. Adv Phys 44:475–588

Stronski A (1998) Production of metallica patterns with the help of high resolution inorganic resists. In: Harman G, Mach P (eds) Micrielectronic interconnections and assembly. NATO ASI series. 3: High technology. Kluwer Academic Publishers, Netherlands, pp 266–293

Stronski AV, Vlcek M (2000) Imaging properties of $As_{40}S_{40}Se_{20}$ layers. Optoelectron Rev 8(3):263–267

Tanaka K (1990) Photoinduced structural changes in chalcogenide glasses. Rev Solid State Sci 4:641–659

Ueno T (1983) Chemical shifts of photoelectron and auger lines in Ag- or Cu-doped amorphous $GeSe_2$ and As_2Se_3. Jpn J Appl Phys 22:1469–1473

Ueno T, Odajima A (1981) X-ray photoelectron spectroscopy of Ag- and Cu-doped amorphous As_2Se_3. Jpn J Appl Phys 20:L501–L504

Wanger CD, Riggs WM, Davis LE, Moulder JF, Muilenberg GE (1979) Handbook of X-ray photoelectron spectroscopy. Physical Electronics Division, Perkin-Elmer Corp, Eden Prairie

Yeh JJ (1993) Atomic Calculation of photoionization cross-sections and asymmetry parameters. Gordon and Breach Science Publishers, Langhorne, PE (USA) and from Yeh JJ and Lindau I (1985) Atomic subshell photoionization cross sections and asymmetry parameters: $1 \leq Z \leq 103$. At Data Nucl Data Tables 32:1–155

Zakery A, Eliiott SR (2007) Optical nonlinearities in chalcogenide glasses and their applications. Springer, Berlin